



HAL
open science

A pseudo-isotropic three phalanxes under-actuated finger

Ghassan Dandash, Rani Rizk, Sébastien Krut, Etienne Dombre

► **To cite this version:**

Ghassan Dandash, Rani Rizk, Sébastien Krut, Etienne Dombre. A pseudo-isotropic three phalanxes under-actuated finger. IFToMM'2011: 13th World Congress in Mechanism and Machine Science, Jun 2011, Guanajuato, Mexico. pp.1-8. lirmm-00643542

HAL Id: lirmm-00643542

<https://hal-lirmm.ccsd.cnrs.fr/lirmm-00643542>

Submitted on 22 Nov 2011

HAL is a multi-disciplinary open access archive for the deposit and dissemination of scientific research documents, whether they are published or not. The documents may come from teaching and research institutions in France or abroad, or from public or private research centers.

L'archive ouverte pluridisciplinaire **HAL**, est destinée au dépôt et à la diffusion de documents scientifiques de niveau recherche, publiés ou non, émanant des établissements d'enseignement et de recherche français ou étrangers, des laboratoires publics ou privés.

A pseudo-isotropic three-phalanx under-actuated finger

G. Dandash*
Lebanese University,
Doctoral School
Hadath, Lebanon

R. Rizk†
Lebanese University,
Doctoral School
Hadath, Lebanon

S. Krut‡
Lirmm, Montpellier 2
University-CNRS
161 rue Ada
Montpellier France

E. Dombre§
Lirmm, Montpellier 2
University-CNRS
161 rue Ada
Montpellier France

Abstract— *A good gripper can adapt itself on any grasped object and ensure contact pressure as homogenous as possible. A gripper that provides a uniform contact pressure is said to be isotropic. Another feature of a gripper is its dexterity, which can be improved by under-actuation. This paper presents the design of a three-phalanx pseudo-isotropic under-actuated finger with anthropomorphic dimensions. Contact forces depend on the gripper folding angles and the transmission torque ratio between unactuated joints. In order to ensure a grasping as isotropic as possible two cams were used. The isotropy is checked up by recalculation of the contact forces.*

Keywords: grasping, under-actuation, fingers, cam-tendon mechanism

Nomenclature

- L_1 , L_2 and L_3 : The proximal, middle and distal phalanx lengths respectively
- I_1 , I_2 and I_3 : contact points between the phalanxes and the grasped object
- P_1 : simple-neck pulley centered at O_1
- P_2 : double-neck pulley centered at O_2 .
- P_3 : simple-neck pulley centered at O_3 and welded to the distal phalanx
- f_1 , f_2 and f_3 contact forces at the proximal, middle and distal phalanxes respectively
- θ_1 : is the angle defining the rotation of the proximal phalanx relatively to the absolute vertical fixed to the frame.
- θ_2 : The angle between the proximal and the middle phalanx
- θ_3 : The angle between the middle and the distal phalanx
- T_a : actuator torque.
- r_1 : radius of P_1
- r_{2i} and r_{2e} internal and external radii of P_2
- r_3 : radius of P_3

* guss_dandash@hotmail.com

† ranyrizk@hotmail.com

‡ krut@lirmm.fr

§ dombre@lirmm.fr

¹ 13th World Congress in Mechanism and Machine Science, Guanajuato, México, 19-25 June, 2011

I Introduction

Grippers are widely used in industry as well as in medicine. They can be used as tools to grasp an object. They can be used also as artificial fingers and hands for amputee people. A gripper is characterized by its dexterity. It has to adapt itself on whatever grasped shape. It has also to grasp with contact forces as homogenous as possible. A bad adaptation leads to the loss of grasping by ejection. A bad contact forces distribution leads to stress concentration then to the worsening of the grasped object. A gripper that provides a uniform contact pressure is said to be isotropic [1]. The best gripper is of course the human hand. However, the closest gripper to the human finger requires more than ten actuators and sensors [2]. The control of such gripper is tricky even with the newest CPU. Moreover, its cost is prohibitive.

Advanced robotic hands have been developed with the isotropy requirement in mind. Many dexterous hands having several actuators (more than six) can be mentioned: the Utah/MIT hand [3], the Stanford/JPL Salisbury's hand [4], the Belgrad hand revisited at USC [5], the DLR hand [6]. The dexterity can also be obtained by under-actuation. The principle consists in equipping the finger with fewer actuators than the number of degrees of freedom (DOF) [7]. Thus, the shape of the grasped object and the static equilibrium govern the gripper configuration. In [8], the advantages of such under-actuated gripper over a simple parallel one are presented. In [9], an under-actuated hand with three fingers is presented. Each finger has two phalanxes and one actuator. A special mechanism is added in order to allow the distal phalanxes to be maintained orthogonal to the palm when precision grasps are performed. An artificial hand mimicking the human hand is presented in [10]. This hand has partially under-actuated fingers. Each finger has three phalanxes. A coupling is introduced between the motion of the middle and distal phalanxes. A drawback of under-actuation is the difficulty of the contact pressure control.

In this paper we present a pseudo-isotropic under-actuated finger. In this finger we use two cams to provide acceptable ratio between contact forces. In section II we present the under-actuation in robotic hands and the

isotropy in grasping. We set up also a review for most grippers presented in the literature. In section III, we present the finger structure. In section IV we carry out a kineto-static analysis for the finger, where we compute the contact forces. In section V, we set up a design for cams that ensure a pseudo-isotropy in the grasping. In section VI, we check-up our isotropy by recalculating the contact grasping forces. We finish the paper by conclusions and opening next challenges.

II Under-actuation and grasping isotropy

The idea behind the under-actuation is to keep the nature laws govern the mechanical device. The objective is to adapt the gripper on the grasped object, without considering the shape. Under-actuation can be realized by using differential, compliant or triggered mechanism. In order to avoid the deterioration of the grasped object, contact pressure must be as homogenous as possible. A hydrostatic pressure induces a Von-Mises stress equal to zero [31]. An object subjected to an isotropic grasping is less exposed to deterioration.

A. Under-actuation in robotic fingers

The concept of under-actuation in robotic hands should not be confused with under-actuation in robotic systems. The joint coordinates of an under-actuated robot are indirectly controllable. The cart and pole system (inverted pendulum) [24] is under-actuated. The pendulum has four DOF among which two are actuated and two are governed by the system dynamics. In an under-actuated finger, joint angles are imposed by the grasped object shape, the static equilibrium and passive components (spring, mechanical limits,...). The main difference between both concepts is that in robotic systems DOF are governed by the dynamics and in robotic fingers by the statics. However, if in robotic systems the number of DOF is the rank of the Jacobian matrix as in the Grübler formula [25], in under-actuated fingers the number of DOF represents the number of parameters that define the finger configuration. These parameters are also called “configuration variables” [15]. The BarrettHand [16] can also be considered as under-actuated since the folding angle of each finger depends not only on the actuator but also on the shape of the grasped object, thus there is one actuator and two DOF. In addition to the classical parameters known in robotics, the notion of kinematic irreversibility and the use of flexible bodies must be introduced. The gripper developed for the Canadian Space Agency is said to have 10 DOF [13], but the backdrivability of each finger has been removed thanks to worm gears. The under-actuated prosthetic hand of Arts Lab (Italy) [14] relies on an “adaptive grasp mechanism” designed to share the forces throughout each finger using compression springs.

Under-actuation can be achieved by using differential, compliant or triggered mechanisms. Differential mechanisms can be based on linkage systems [2, 7, 8, 10, 13, 22] or on tendon-actuated mechanisms [1, 9, 11, 12, 15, 17, 20, 21, 22]. Tendon systems are limited to small grasp forces. They induce friction and elasticity. Linkage mechanisms are more efficient for applications with large grasp forces but are relatively more bulky.

In triggered mechanisms, once the torque exceeds a certain value, the joint locks. On the BarrettHand, the transmission is disengaged and an irreversible mechanism prevents backdrivability of the joint [18]. In Lee's hand [19], this is achieved by the use of automatic brakes.

It is also possible to reduce the number of actuators by introducing compliance for each DOF. In [14], each finger is linked to a common actuator through compliant springs. If one of the fingers is blocked, the other ones are not blocked for a certain range. The stiffness of the springs must be sufficiently small in order to allow adaptation. Therefore, the stiffness of the grasp is limited.

Differential mechanisms allow control of the contact forces on the phalanxes in contact, but require high actuator torques and high internal loads in the gripper structure, as they guarantee conditional grasp stability only. Compliant mechanisms are capable of adapting themselves to the shape of the grasped object and are always in equilibrium, but if contact forces depend on spring stiffness then they are non-controllable. Triggered mechanisms provide always a stable grasp on a fixed object since there is no sliding, but they are not able to follow a moving object once the contact with this object is lost since the motion of the proximal phalanx is blocked.

Robotic or prosthetic fingers in which the motion of all phalanxes is mechanically coupled [23, 29, 30] are not under-actuated. They have one actuator and one DOF. The motion is determined by the design and there is no shape adaptation.

B. Force isotropy

Large differences between contact forces induce bad stress-distribution on the grasped object, meaning bad distribution of deformation, and consequently stress-concentration and deterioration. It is known that a hydrostatic pressure induces a Von-Mises stress null [31]. Hence a body subjected to hydrostatic pressure does not present any risk of deterioration. A gripper which ensures uniform contact pressure is said to be “isotropic” [1]. In [20] a gripper which ensures the same contact force on the middle of each phalanx is presented. Since both phalanxes have the same length, it is possible to consider the gripper as isotropic. This is true since the contact force is the resultant of the uniform pressure exerted on

the phalanx. In our case, the goal is to design a pseudo-isotropic three-phalanx finger with anthropomorphic dimensions. In human fingers, the distances between the rotational axes of the phalanxes are variable. The mean distance between the rotational axes of the first phalanx is equal to the sum of the distance between the rotational axes of the middle phalanx and the length of the distal phalanx [23]. In other words, the mean length of the first phalanx is equal to the sum of the lengths of the two other phalanxes. If we consider this property valid for n phalanxes, the ratio between the lengths of two consecutive phalanxes should be the “golden ratio”, thus:

$$l_3 = \beta l_2 = \beta^2 l_1 \quad (1)$$

$$\beta = \frac{\sqrt{5}-1}{2}$$

The phalanxes are of different lengths. When the finger is subjected to a uniform linear pressure p , the resultant force on each phalanx is the product of p and the length of the phalanx. In the ideal case, forces f_1 , f_2 and f_3 exerted respectively on the proximal, middle and distal phalanxes are:

$$f_1 = pl_1 \quad f_2 = pl_2 = \frac{1}{\beta} f_1 \quad f_3 = pl_3 = \left(\frac{1}{\beta}\right)^2 f_1 \quad (2)$$

In conclusion, the aim is to find mechanisms for torque transmission that ensures contact forces, the closest to those computed in (2).

III Finger structure

In a pulley-tendon finger, the torque transmission ratios are equal to the pulley radius ratios [2]. The idea is to replace the pulleys by cams [20] in order to give variable transmission ratio depending on the folding angle, hence ensuring force isotropy.

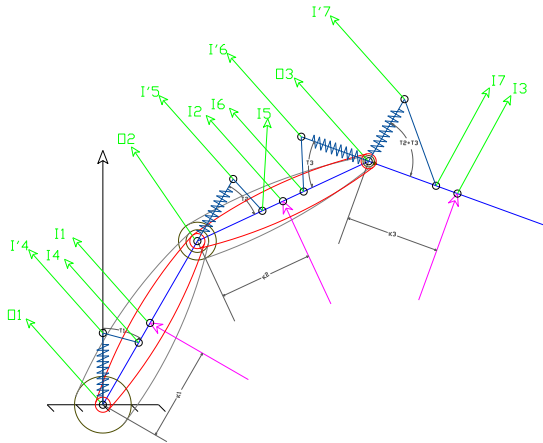


Fig. 1. Finger kinematic structure

The contact force is assumed as the resultant of a uniform pressure. Then, the contact points are considered to be in the middle of corresponding phalanxes, thus (figure 1):

$$O_1I_1 = K_1 = L_1/2 \quad O_2I_2 = K_2 = L_2/2 \quad O_3I_3 = K_3 = L_3/2 \quad (3)$$

A system of springs pulls back the finger once the actuator is relaxed. The effect of these springs is neglected in the following, because the springs are with low stiffness and their torques are negligible. The system of pulleys used in the finger includes 2 simple-neck pulleys and 1 double-neck pulley. The actuator turns the pulley P_1 centered at O_1 . Due to a tendon the actuator torque is reduced and transmitted to the double neck pulley P_2 . Another tendon transmits the torque to the third pulley P_3 . P_3 is welded to the third phalanx. Then, the rotation of P_3 drives the distal phalanx.

IV Kineto-static analysis of the finger

Contact forces are mainly function of the folding angles and transmission ratios. The problem consists in finding the transmission ratios that ensure isotropy. Then we have to find the profiles of cams that ensure these transmission ratios. Based on the virtual work theorem we can compute the grasping forces. It is a matter to establish a balance between the powers, produced by the actuator P_a and consumed by the contact forces T_f . These powers are balanced at equilibrium. The produced power is simply:

$$P_a = T_a \dot{\theta}_a \quad (4)$$

$\dot{\theta}_a$ is the virtual rotational velocity of the actuator.

To compute the consumed power P_f , we need the contact points, I_1 , I_2 and I_3 , velocities. Indeed, the contact point positions are given by the vectors:

$$\begin{aligned} \overline{O_1I_1} &= K_1 \begin{bmatrix} -\sin \theta_1 \\ \cos \theta_1 \end{bmatrix} \\ \overline{O_1I_2} &= \overline{O_1O_2} + \overline{O_2I_2} \\ &= L_1 \begin{bmatrix} -\sin \theta_1 \\ \cos \theta_1 \end{bmatrix} + K_2 \begin{bmatrix} -\sin(\theta_1 + \theta_2) \\ \cos(\theta_1 + \theta_2) \end{bmatrix} \\ \overline{O_1I_3} &= \overline{O_1O_2} + \overline{O_2O_3} + \overline{O_3I_3} \\ &= L_1 \begin{bmatrix} -\sin \theta_1 \\ \cos \theta_1 \end{bmatrix} + L_2 \begin{bmatrix} -\sin(\theta_1 + \theta_2) \\ \cos(\theta_1 + \theta_2) \end{bmatrix} + K_3 \begin{bmatrix} -\sin(\theta_1 + \theta_2 + \theta_3) \\ \cos(\theta_1 + \theta_2 + \theta_3) \end{bmatrix} \end{aligned} \quad (5)$$

To get the velocities, we need to derivate the positions with respect to the time:

$$\begin{aligned} \overline{v_1} &= k_1 \begin{bmatrix} -\cos \theta_1 \cdot \dot{\theta}_1 \\ -\sin \theta_1 \cdot \dot{\theta}_1 \end{bmatrix} \\ \overline{v_2} &= L_1 \begin{bmatrix} -\cos \theta_1 \cdot \dot{\theta}_1 + K_2 \begin{bmatrix} -\cos(\theta_1 + \theta_2)(\dot{\theta}_1 + \dot{\theta}_2) \\ -\sin(\theta_1 + \theta_2)(\dot{\theta}_1 + \dot{\theta}_2) \end{bmatrix} \\ -\sin \theta_1 \cdot \dot{\theta}_1 \end{bmatrix} \\ \overline{v_3} &= L_1 \begin{bmatrix} -\cos \theta_1 \cdot \dot{\theta}_1 + L_2 \begin{bmatrix} -\cos(\theta_1 + \theta_2)(\dot{\theta}_1 + \dot{\theta}_2) \\ -\sin(\theta_1 + \theta_2)(\dot{\theta}_1 + \dot{\theta}_2) \end{bmatrix} \\ -\sin \theta_1 \cdot \dot{\theta}_1 \end{bmatrix} \\ &\quad + K_3 \begin{bmatrix} -\cos(\theta_1 + \theta_2 + \theta_3)(\dot{\theta}_1 + \dot{\theta}_2 + \dot{\theta}_3) \\ -\sin(\theta_1 + \theta_2 + \theta_3)(\dot{\theta}_1 + \dot{\theta}_2 + \dot{\theta}_3) \end{bmatrix} \end{aligned} \quad (6)$$

Contact forces are normal to the phalanxes. They are given by the vectors:

$$\begin{aligned}\bar{f}_1 &= f_1 \begin{bmatrix} -\cos \theta_1 \\ -\sin \theta_1 \end{bmatrix} \\ \bar{f}_2 &= f_2 \begin{bmatrix} -\cos(\theta_1 + \theta_2) \\ -\sin(\theta_1 + \theta_2) \end{bmatrix} \\ \bar{f}_3 &= f_3 \begin{bmatrix} -\cos(\theta_1 + \theta_2 + \theta_3) \\ -\sin(\theta_1 + \theta_2 + \theta_3) \end{bmatrix}\end{aligned}\quad (7)$$

and the consumed power P_f is:

$$\begin{aligned}P_f &= \bar{f}_1 \cdot \bar{v}_1 + \bar{f}_2 \cdot \bar{v}_2 + \bar{f}_3 \cdot \bar{v}_3 = \\ &k_1 f_1 \dot{\theta}_1 + L_1 f_2 \cos(\theta_2) \dot{\theta}_1 + k_2 f_2 (\dot{\theta}_1 + \dot{\theta}_2) \\ &+ L_1 f_3 \cos(\theta_2 + \theta_3) \dot{\theta}_1 + L_2 f_3 \cos(\theta_3) (\dot{\theta}_1 + \dot{\theta}_2) \\ &+ f_3 k_3 (\dot{\theta}_1 + \dot{\theta}_2 + \dot{\theta}_3)\end{aligned}\quad (8)$$

what can be written in the form:

$$\begin{aligned}P_f &= [f]^T T [\dot{\theta}] \\ T &= \begin{bmatrix} k_1 & 0 & 0 \\ L_1 \cos \theta_2 + k_2 & k_2 & 0 \\ L_1 \cos(\theta_2 + \theta_3) + L_2 \cos \theta_3 + k_3 & L_2 \cos \theta_3 + k_3 & k_3 \end{bmatrix} \\ [f] &= [f_1 \quad f_2 \quad f_3]^T \quad [\dot{\theta}] = [\dot{\theta}_1 \quad \dot{\theta}_2 \quad \dot{\theta}_3]^T\end{aligned}\quad (9)$$

On the other hand we have [22]:

$$\dot{\theta}_a = \begin{bmatrix} 1 & \frac{r_{2i}}{r_1} & \frac{r_{2i}}{r_1} \frac{r_3}{r_{2e}} \\ \frac{r_{2i}}{r_1} & \frac{r_{2i}}{r_1} & \frac{r_{2i}}{r_1} \frac{r_3}{r_{2e}} \\ \frac{r_{2i}}{r_1} & \frac{r_{2i}}{r_1} & \frac{r_{2i}}{r_1} \frac{r_3}{r_{2e}} \end{bmatrix} \begin{bmatrix} \dot{\theta}_1 \\ \dot{\theta}_2 \\ \dot{\theta}_3 \end{bmatrix}.\quad (10)$$

The power balance gives:

$$P_a = T_a \dot{\theta}_a = T_a \begin{bmatrix} 1 & \frac{r_{2i}}{r_1} & \frac{r_{2i}}{r_1} \frac{r_3}{r_{2e}} \end{bmatrix} [\dot{\theta}] = [f]^T T [\dot{\theta}]\quad (11)$$

Then we get:

$$\begin{aligned}T_a \begin{bmatrix} 1 & \frac{r_{2i}}{r_1} & \frac{r_{2i}}{r_1} \frac{r_3}{r_{2e}} \end{bmatrix} &= \\ \begin{bmatrix} f_1 \\ f_2 \\ f_3 \end{bmatrix}^T \begin{bmatrix} k_1 & 0 & 0 \\ L_1 \cos \theta_2 + k_2 & k_2 & 0 \\ L_1 \cos(\theta_2 + \theta_3) + L_2 \cos \theta_3 + k_3 & L_2 \cos \theta_3 + k_3 & k_3 \end{bmatrix} &\end{aligned}\quad (12)$$

and then:

$$\begin{aligned}f_1 &= \frac{T_a}{k_1} \left[1 - \frac{r_{2i}}{r_1 k_2} (L_1 \cos \theta_2 + k_2) + A \right] \\ A &= \frac{r_{2i} r_3}{r_1 r_{2e} k_3} \left\{ \frac{L_1}{k_2} \cos \theta_2 (L_2 \cos \theta_3 + k_3) - L_1 \cos(\theta_2 + \theta_3) \right\} \\ f_2 &= \frac{T_a}{k_2} \left[\frac{r_{2i}}{r_1} - \frac{r_{2i} r_3}{r_1 r_{2e} k_3} (L_2 \cos \theta_3 + k_3) \right] \\ f_3 &= \frac{T_a r_{2i} r_3}{k_3 r_1 r_{2e}}\end{aligned}\quad (13)$$

As equation (13) gives the distal force free of folding angles, the middle force depends on θ_3 and the proximal force depends on θ_2 and θ_3 simultaneously. In [20] a cam was used to create isotropy between two contact forces. A cam is a pulley with variable radius of curvature. The radius of curvature of a curve depends on one variable only. That is why we cannot use a planar cam to create isotropy in a three-phalanx under-actuated finger. In the following, we will try to find a cam that ensures a pseudo isotropy in the grasping.

V Cam design

A gripper can be assumed isotropic if it provides contact forces proportional to the lengths of its phalanxes. We are looking for the ratio computed in equation (2), which leads to:

$$f_3 = \beta f_2 = \beta^2 f_1.\quad (14)$$

By replacing f_1 , f_2 and f_3 by their values we get:

$$\begin{aligned}\frac{k_2 r_3}{k_3 r_{2e}} &= \beta \left(1 - \frac{r_3}{r_{2e}} - \frac{r_3 L_2}{r_{2e} k_3} \cos \theta_3 \right) \\ \Rightarrow \frac{r_3}{r_{2e}} \left[\frac{k_2}{k_3} + \beta \left(1 + \frac{L_2}{k_3} \cos \theta_3 \right) \right] &= \beta \\ \Rightarrow R = \frac{r_3}{r_{2e}} = \frac{\beta}{\frac{1}{\beta} + \beta + 2 \cos \theta_3}\end{aligned}\quad (15)$$

And:

$$\begin{aligned}\frac{T_a}{k_2} \left(\frac{r_{2i}}{r_1} - \frac{r_{2i} r_3}{r_1 r_{2e}} - \frac{r_{2i} r_3 L_2}{r_1 r_{2e} k_3} \cos \theta_3 \right) &= \beta \frac{T_a}{k_1} \left[1 - \frac{L_1 r_{2i}}{k_2 r_1} \cos \theta_2 - \frac{r_{2i}}{r_1} + A \right] \\ \Rightarrow \frac{k_1}{k_2} \frac{r_{2i}}{r_1} (1 - R - R \frac{L_2}{k_3} \cos \theta_3) &= \beta \left[1 - \frac{L_1 r_{2i}}{k_2 r_1} \cos \theta_2 - \frac{r_{2i}}{r_1} + A \right]\end{aligned}\quad (16)$$

(A is defined in equation (13)).

That gives:

$$\begin{aligned}R_1 = \frac{r_{2i}}{r_1} &= \frac{\beta}{\beta + \frac{1}{\beta} - \frac{R}{\beta} - \frac{2R}{\beta^2} \cos \theta_3 + B} \\ B &= 2 \cos \theta_2 - 2R \cos \theta_2 - \frac{4R}{\beta} \cos \theta_2 \cos \theta_3 + \frac{2R}{\beta} \cos(\theta_2 + \theta_3)\end{aligned}\quad (17)$$

These formulas define the transmission ratios $R = r_3/r_{2e}$ and $R_1 = r_{2i}/r_1$. Using the ratio R we can straightforwardly get the profile of the cam between the middle and the distal phalanx [20]. The problem is to find the cam that gives the right reduction ratio between the torque T_a and the torque T_2 applied on the pulley P_2 . This ratio is R_1 . To get it, we need r_{2i} , the lever arm for the tendon, function of θ_2 and θ_3 simultaneously. This goal is not easy to reach. That is why we will discretize θ_3 . For each value of θ_3 we will compute the profile of the cam when θ_2 varies that gives us the well transmission ratio. Finally

we will take the average profile of all the obtained profiles.

However the problem is a little bit more complicated than the first case (between the middle and distal phalanxes). In fact, in the first case P_3 was welded to the distal phalanx and θ_3 gives the rotation of P_3 with respect to the middle phalanx. Now the pulley P_2 is free and the profile should be computed as a function of θ_{2p}^r (the rotation of P_2 with respect to the proximal phalanx).

In order to be able to sketch the profile for the cam used in P_2 we need the ratio R_1 function of θ_{2p}^r . We know [2]:

$$\begin{aligned} \dot{\theta}_{2p}^r - R\dot{\theta}_3 &= \dot{\theta}_2 \\ \Rightarrow d\theta_{2p}^r - \frac{\beta d\theta_3}{\beta + \frac{1}{\beta} + 2\cos\theta_3} &= d\theta_2 \\ \Rightarrow \theta_2 &= \theta_{2p}^r - f(\theta_3) \end{aligned} \quad (18)$$

$$f(\theta_3) = 2\beta \tan^{-1} \left(\frac{\sqrt{\left(\beta + \frac{1}{\beta}\right)^2 - 4} \tan\left(\frac{\theta_3}{2}\right)}{\beta + \frac{1}{\beta}} \right)$$

Let assume that $\theta_{2p}^r = 0$ when $\theta_2 = \theta_3 = 0$. Then:

$$\begin{aligned} r_{2i} &= \frac{U}{V} \\ U &= r_1\beta \\ V &= \beta + \frac{1-R}{\beta} - \frac{2R}{\beta^2} \cos\theta_3 + 2(1-R)\cos(\theta_{2p}^r - f(\theta_3)) \\ &\quad - \frac{4R}{\beta} \cos(\theta_{2p}^r - f(\theta_3))\cos\theta_3 + \frac{2R}{\beta} \cos(\theta_{2p}^r - f(\theta_3) + \theta_3) \end{aligned} \quad (19)$$

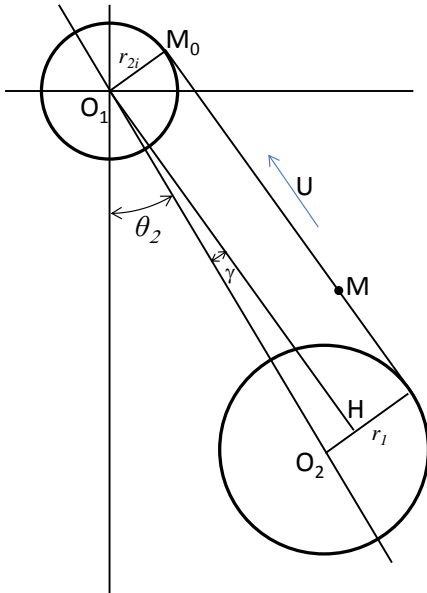


Fig. 2. Cam tendon system

Equation (19) gives the lever arm of the tendon force with respect to O_2 function of θ_{2p}^r and θ_3 . r_{2i} is simply the distance between O_2 and the tendon. A rotation of P_2 by an angle θ_{2p}^r with respect to the proximal phalanx is equivalent to a rotation of the phalanx by an angle $-\theta_{2p}^r$ with respect to P_2 (Figure 2). Mathematically the tendon can be modeled by a line. For given values of θ_{2p}^r and θ_3 the line is at a distance r_{2i} of O_2 and r_1 of O_1 . We will consider n discret values for θ_3 between 0 and $\pi/2$. For each value θ_{3i} of θ_3 ($i=1 \dots n$), we consider the set of lines defined by the variation of θ_2 between 0 and $\pi/2$. The envelope curve of this set of lines is the cam that provides isotropy for this special value θ_{3i} (figure 3).

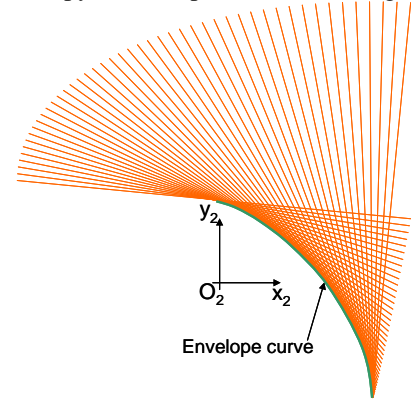


Fig. 3. Envelope curve

Let γ be the angle between O_1O_2 and the tendon. The geometry gives:

$$\sin\gamma = \frac{O_1H}{L_1} = \frac{r_1 - r_{2i}}{L_1} \quad (20)$$

Let M_0 the nearest point of the tendon to O_2 . It is described by the vector:

$$\overline{O_2M_0} = \begin{bmatrix} r_{2i} \cos(\gamma + \theta_{2p}^r) \\ r_{2i} \sin(\gamma + \theta_{2p}^r) \end{bmatrix} \quad (21)$$

Let M be any point of the tendon. It is described by the vector:

$$\overline{O_2M} = \overline{O_2M_0} + \lambda \vec{u} \quad (22)$$

Where \vec{u} is the unit vector of the tendon and λ is a real parameter. Therefore we have:

$$\overline{O_2M} = \begin{bmatrix} r_{2i} \cos(\gamma + \theta_{2p}^r) + \lambda \cos\left(\frac{\pi}{2} + \gamma + \theta_{2p}^r\right) \\ r_{2i} \sin(\gamma + \theta_{2p}^r) + \lambda \sin\left(\frac{\pi}{2} + \gamma + \theta_{2p}^r\right) \end{bmatrix} \quad (23)$$

Equation [23] is the equation of a set of lines. We have to derivate the vector $\overline{O_2M}$ with respect to λ and to θ_{2p}^r . The envelope curve is gotten by the values of λ that give:

$$\det\left(\frac{\delta \overline{O_2M}}{\delta \theta_{2p}^r}; \frac{\delta \overline{O_2M}}{\delta \lambda}\right) = 0 \quad (24)$$

$$\frac{\delta \overline{O_2 M}}{\delta \lambda} = \begin{cases} \cos\left(\frac{\pi}{2} + \gamma + \theta_{2p}^r\right) = -\sin(\gamma + \theta_{2p}^r) \\ \sin\left(\frac{\pi}{2} + \gamma + \theta_{2p}^r\right) = +\cos(\gamma + \theta_{2p}^r) \end{cases} \quad (25)$$

And:

$$\frac{\delta \overline{O_2 M}}{\delta \theta_{2p}^r} = \begin{cases} r_{2i}^r \cos(\gamma + \theta_{2p}^r) - r_{2i} \sin(\gamma + \theta_{2p}^r)(\gamma' + 1) \\ -\lambda(\gamma' + 1) \sin\left(\frac{\pi}{2} + \gamma + \theta_{2p}^r\right) \\ r_{2i}^r \sin(\gamma + \theta_{2p}^r) + r_{2i} \cos(\gamma + \theta_{2p}^r)(\gamma' + 1) \\ +\lambda(\gamma' + 1) \cos\left(\frac{\pi}{2} + \gamma + \theta_{2p}^r\right) \end{cases} \quad (26)$$

so:

$$\begin{bmatrix} -\sin(\gamma + \theta_{2p}^r) & E \\ \cos(\gamma + \theta_{2p}^r) & F \end{bmatrix} = 0 \quad (27)$$

then:

$$\sin(\gamma + \theta_{2p}^r)E + \cos(\gamma + \theta_{2p}^r)F = 0$$

$$E = r_{2i}^r \sin(\gamma + \theta_{2p}^r) + r_{2i} \cos(\gamma + \theta_{2p}^r)(\gamma' + 1) + \lambda(\gamma' + 1) \cos\left(\frac{\pi}{2} + \gamma + \theta_{2p}^r\right) \quad (28)$$

$$F = r_{2i}^r \cos(\gamma + \theta_{2p}^r) - r_{2i} \sin(\gamma + \theta_{2p}^r)(\gamma' + 1) - \lambda(\gamma' + 1) \sin\left(\frac{\pi}{2} + \gamma + \theta_{2p}^r\right)$$

$$\Rightarrow [r_{2i}^r \sin^2(\gamma + \theta_{2p}^r) + r_{2i} \sin(\gamma + \theta_{2p}^r) \cos(\gamma + \theta_{2p}^r)(\gamma' + 1) - \lambda(\gamma' + 1) \sin^2(\gamma + \theta_{2p}^r)] + [r_{2i}^r \cos^2(\gamma + \theta_{2p}^r) - r_{2i} \cos(\gamma + \theta_{2p}^r) \sin(\gamma + \theta_{2p}^r)(\gamma' + 1) - \lambda(\gamma' + 1) \cos^2(\gamma + \theta_{2p}^r)] = 0 \quad (29)$$

$$\Rightarrow r_{2i}^r - \lambda(\gamma' + 1) = 0 \quad (30)$$

$$\lambda = \frac{r_{2i}^r}{(\gamma' + 1)} \quad (31)$$

$$\Rightarrow \frac{1}{\lambda} = \frac{(\gamma' + 1)}{r_{2i}^r}$$

In other words we have:

$$\frac{1}{\lambda} = \frac{\frac{\partial \gamma}{\partial \theta_{2p}^r} + 1}{\frac{\partial r_{2i}^r}{\partial \theta_{2p}^r}} = \frac{\partial \gamma}{\partial r_{2i}^r} + \frac{1}{\frac{\partial r_{2i}^r}{\partial \theta_{2p}^r}} \quad (32)$$

But equation (20) gives:

$$r_{2i} = r_1 - L_1 \sin \gamma \Rightarrow \frac{\partial r_{2i}}{\partial \gamma} = -L_1 \cos \gamma \quad (33)$$

The derivative of equation (19) gives:

$$\frac{\partial r_{2i}}{\partial \theta_{2p}^r} = \frac{U'V - UV'}{V^2} \quad (34)$$

(This derivative is taken for a special value of θ_3 and the derivative of θ_3 is zero)

$$U' = 0$$

$$V' = -2(1-R) \sin(\theta_{2p}^r - f(\theta_3)) + \frac{2R}{\beta} \left(2 \cos \theta_3 \sin(\theta_{2p}^r - f(\theta_3)) - \sin(\theta_{2p}^r - f(\theta_3) + \theta_3) \right) \quad (35)$$

then:

$$\lambda = \frac{L_1 \beta r_1 V' \cos \gamma}{V^2 L_1 \cos \gamma - \beta r_1 V'} \quad (36)$$

If we replace λ in the equation (23) we get:

$$\overline{O_2 M} = \begin{cases} r_{2i} \cos(\gamma + \theta_{2p}^r) - \frac{L_1 \beta r_1 V' \cos \gamma}{V^2 L_1 \cos \gamma - \beta r_1 V'} \sin(\gamma + \theta_{2p}^r) \\ r_{2i} \sin(\gamma + \theta_{2p}^r) + \frac{L_1 \beta r_1 V' \cos \gamma}{L_1 V^2 \cos \gamma - \beta r_1 V'} \cos(\gamma + \theta_{2p}^r) \end{cases} \quad (37)$$

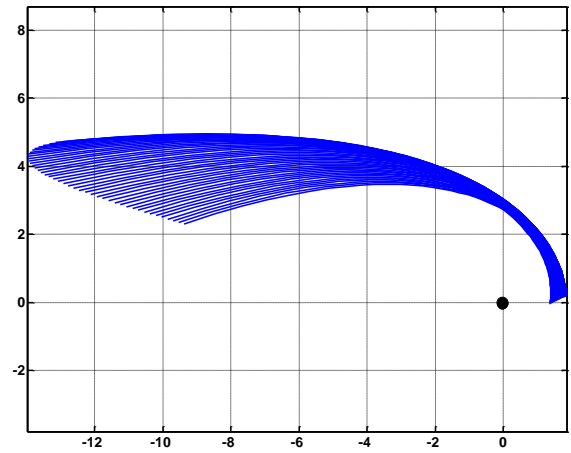


Fig. 4. Cam profiles for different values of θ_3

We get a set of cams. Each cam corresponds to a special value of θ_3 and its corresponding value of r_3 . The profiles for $r_1=7.5\text{mm}$, $r_{2e}=5\text{mm}$ and $L_1=50\text{mm}$ are shown in figure 4.

The coordinates X and Y of the vector $\overline{O_2 M}$ are in reality $X(\theta_{3i})$ and $Y(\theta_{3i})$. For our finger, we will take the average cam on θ_3 . Then the profile of the cam is given by:

$$\bar{X} = \frac{\sum_{i=1}^n X(\theta_{3i})}{n} \quad (38)$$

$$\bar{Y} = \frac{\sum_{i=1}^n Y(\theta_{3i})}{n}$$

The average cam profile is shown in figure 5:

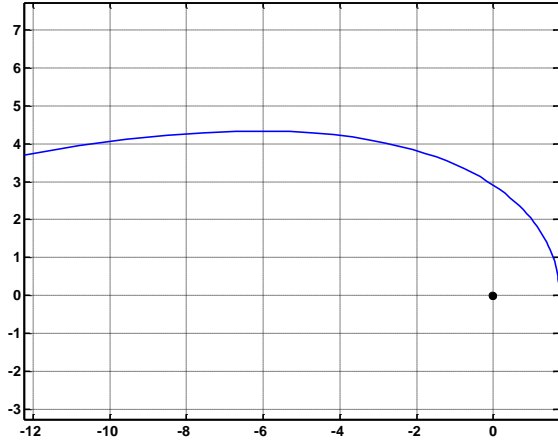


Fig. 5: Average cam profile

In conclusion, thanks to the envelope curve, we found for each value of θ_3 a cam. This cam ensures isotropy when the middle phalanx folds alone. In order to get isotropy everywhere we need to choose the right cam for each value of θ_3 . The average cam found in this paragraph provides for a given value of θ_2 the average transmission ratio when θ_3 varies from 0 to $\pi/2$. The grasping gotten is not perfectly isotropic but it is pseudo-isotropic. To check up the isotropy, we need to recalculate the grasping forces.

VI Forces recalculation according to the average cam

After the use of the average cam, the recalculation of the value of the forces f_1, f_2 and f_3 is a necessity to specify to which limit the force isotropy was lost and to define whether this limit is acceptable or not. The only difference imposed by the use of the average cam that can affect f_1, f_2 and f_3 is the value of the internal 2nd pulley (cam) radius r_{2i} . Therefore, we have to recalculate r_{2i} according to the new average cam profile then replace its value in f_1, f_2 and f_3 .

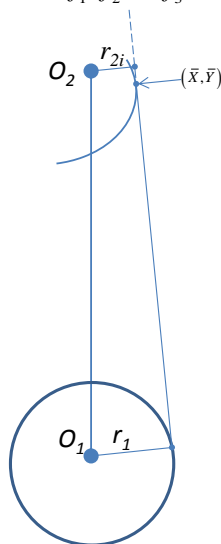


Fig. 6: recalculation of r_{2i}

For each value of θ_{2p}^r , we know the coordinates (\bar{X}, \bar{Y}) of the point of tangency to the cam. The slope of the line is computed numerically, by computing the derivatives of \bar{X} and \bar{Y} with respect to θ_{2p}^r . We have then the equation for the support line of tendon. The value of r_{2i} , can be the minimum distance between O_2 and the tendon (figure 6) Once r_{2i} is known we can replace its new value in f_1, f_2 and f_3 and recalculate the forces new ratios in order to specify the limit to which the isotropy was lost. The results can be clearly visualized in the 3-D surface scans of figure 7:

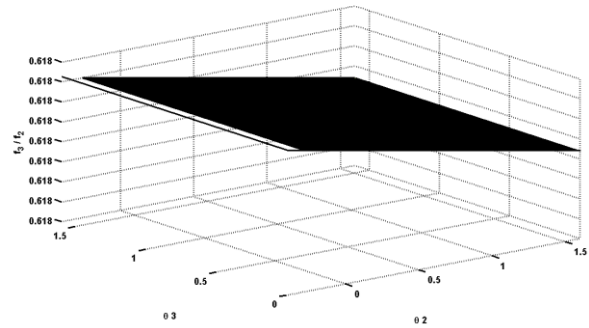


Fig. 7: Ratio f_3/f_2

This surface shows perfect isotropy conservation between f_2 & f_3 . It was predictable since at P_3 we need only one cam to ensure this isotropy.

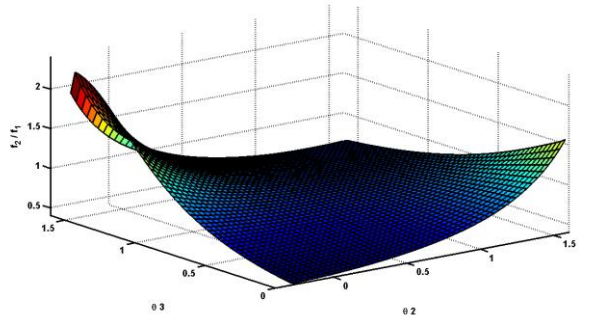


Fig. 8: ratio f_2/f_1

Figure 8 depicts the variation of the ratio f_2/f_1 in the joint space. Ideally this ratio should be equal to 0.618 everywhere (see eq. [1]). The graph shows a smooth variation in the center of the space. The ratio becomes greater than one for a high difference between folding angles. However, even with the human finger, this case is approximately non used. In conclusion to get perfect isotropy we need a complicated mechanism that adjusts the right reduction ratios. With our solution we got an acceptable grasping with a great simplification.

VII Conclusions and further works

In this paper we have proposed a method to design a three-phalanx pseudo-isotropic under-actuated finger. We have carried out a detailed kineto-static analysis. We

have elicited the contact forces. The distal force depends on the distal transmission ratio (at P_3 only). It is independent from the folding angles. The middle force depends on the first transmission ratio (at P_2). It depends also on the folding angle θ_3 . A cam have been used instead P_3 . This cam insures perfect isotropy between the middle and distal phalanxes. The proximal force depends on both folding angles,, and then on two parameters. We have found a set of cams that should be used to ensure perfect isotropy. However, the use of a set of cams is very complicated, that is why we have proposed to make use of the average cam of the set even though it does not provide perfect isotropy. In order to verify our idea, we carried out a recalculation of the contact forces with the cams used. The recalculation has shown a perfect isotropy between the middle and distal phalanxes. On the other hand there is an acceptable trade-off in the center on the joint space. The critical values are in the non used field. To summarize, a great simplification has led to a very acceptable result.

To get a perfect isotropy we would need a sort of gear box to choose the right cam function of θ_3 . Moreover the under-actuation has the drawback to providing conditional stability only, thus a grasp stability analysis should be carried out for this finger. In this paper, the forces developed by the springs were ignored. This assumption holds as long as the stiffness of the spring is very low. In order to be more accurate the spring stiffness should be taken into consideration, which will change the shape of the cam. Another weak point of such mechanisms is the high internal forces mainly in the tendons. These forces should be studied for safe dimensioning purpose. Finally, of course the best validation of our work will be done with a real prototype.

References

- [1] Hirose S. and Umetani Y., "The development of soft gripper for the versatile robot hand", *Mechanism and Machine Theory*, Vol. 13, pp. 351-358, 1978.
- [2] Birglen L. and Gosselin C., "Optimal Design of 2-Phalanx Under-actuated Fingers", in Proc. of International Conference on Intelligent Manipulation and Grasp, pp. 110-116, Genoa, Italy, July 1-2, 2004
- [3] Jacobsen S. C., Iversen E. K., Knutti D. F., Johnson R. T., and Biggers K. B., "Design of the UTAH/MIT dextrous hand", in Proc. of ICRA86, San Francisco, CA, USA, 1986, pp. 1520-1532.
- [4] Salisbury J. K. and Craig J. J., "Articulated hands: Force control and kinematic issues", *The International Journal of Robotics Research*, Vol. 1, No. 1, pp. 4-17, 1982.
- [5] Bekey G. A., Tomovic R., and Zeljkovic I., "Control Architecture for the Belgrade/USC Hand in Dextrous Robot Hands", Springer-Verlag, New York, 1999.
- [6] Butterfass J., Grebenstein M., Liu H., and Hirzinger G., "DLR-hand II: Next generation of a dextrous robot hand", in Proc. of ICRA 2001, Seoul, Korea, May 21-26 2001, pp. 109-114.
- [7] Laliberté T., Birglen L. and Gosselin C., "Under-actuation in robotic grasp hands," *Japanese Journal of Machine Intelligence and Robotic Control*, Special Issue on Under-actuated Robots, vol. 4, no. 3, pp. 77-87, September 2002.
- [8] Shimojima H., Yamamoto K. and Kawawita K., "A Study of Grippers with Multiple Degrees of Mobility," *JSME International Journal*, Vol. 30, No. 261, pp. 515-522, 1987.
- [9] Bartholet S.J., "Reconfigurable End Effector," U.S. Patent 5 108 140, 1992.
- [10] Crowder R.M. and Whatley D.R., "Robotic Gripping Device Having Linkage Actuated Finger Sections," U.S. Patent 4 834 443, 1989.
- [11] Bicchi A. and Kumar V., "Robotic grasp and contact: A review," in Proc. of ICRA2000, San Francisco, CA, USA, 2000.
- [12] Fukaya N., Toyama S., Asfour T. and Dillmann R., "Design of the TUAT/Karlsruhe Humanoid Hand", in IROS 2000, Takamatsu, Japan, October 30 - November 5, 2000.
- [13] Laliberté T. and Gosselin C., "Actuation System for Highly Under-actuated Gripping Mechanism", United States Patent, No. US 6,505,870 B1, January 14, 2003.
- [14] Massa B., Roccella S., Carrozza M. C. and Dario P., "Design and Development of an Under-actuated Prosthetic Hand", in Proc. of ICRA2002, Washington, DC, May 2002.
- [15] Olfati-Saber R., "Nonlinear Control of Under-actuated Mechanical Systems with Application to Robotics and Aerospace Vehicles", Ph.D. Thesis, Department of Electrical Engineering and Computer Science, Massachusetts Institute of Technology, Cambridge, MA, February 2001.
- [16] Townsend W.T., "The BarrettHand grasper - programmably flexible part handling and assembly", *Industrial Robot: An International Journal*, MCB University Press, Vol. 27, No. 3, pp. 181-188, 2000.
- [17] Zhang W., Chen Q., Sun Z. and Zhao D., "Under-actuated passive adaptive grasp humanoid robot hand with control of grasp force", in Proc. of ICRA2003, Taipei, Taiwan, September 14-19, 2003.
- [18] Ulrich N. T., "Methods and Apparatus for Mechanically Intelligent Grasp", United State Patent, No. US 4,957,320, 1988.
- [19] Lee S., "Artificial Dexterous Hand", United States Patent, No. US 4,946,380, August 7, 1990.
- [20] Krut S., "A Force-Isotropic Under-actuated Finger", *Proceeding of the 2005 IEEE, International Conference of the robotics and automation*, Barcelona, Spain, April 2005
- [21] Hirose S., "Connected Differential Mechanism and its Applications", in Proc. of ICAR85, Tokyo, Japan, September 1985.
- [22] Birglen L., "Analysis and control of under-actuated robotic hand", Ph.D. thesis, university Laval, Quebec Canada.
- [23] Eduardo N., Rodriguez N., Carbone G., Ceccarelli M., "Optimal design of driving in a 1-DOF anthropomorphic finger", *Mechanism and Machine Theory*, 2006, Vol 41, p897-911
- [24] Olfati-Saber R., "Fixed Point Controllers and Stabilization of the Cart-Pole System and the Rotating Pendulum", *proc. of the 38th Conference on Decision and Control*, pp. 1174-1181, Phoenix, AZ, Dec. 1999.
- [25] Hunt K.H., *Kinematic Geometry of Mechanisms*, Clarendon Press, Oxford, 1978.
- [26] Crisman J.D., Kanojia C. and Zeid I., "Graspar : A Flexible, Easily Controllable Robotic Hand," *IEEE Robotics and Automation Magazine*, pp. 32-38, June 1996.
- [27] Graham D.F., "Artificial Hand and Digit Therefor," U.S. Patent 5 200 679, 1993.
- [28] Dechev N., Cleghorn W.L. and Naumann S., "Multiple Finger, Passive Adaptive Grasp Prosthetic Hand," *Mechanism and Machine Theory*, Vol. 36, No. 10, pp. 1157-1173, 2001.
- [29] Zhang J., Guo G. and Gruver W.A., "Optimal Design of a Six- Bar Linkage for an Anthropomorphic Three-Jointed Finger Mechanism," *Proceedings of the ASME Mechanisms Conference*, Phoenix, vol. DE-45, pp. 299-304, 1992.
- [30] Haulin E.N., Lakis A.A. and Vinet R., "Optimal Synthesis of a Planar Four-Link Mechanism Used in a Hand Prosthesis," *Mechanism and Machine Theory*, Vol. 36, Nos. 11-12, pp. 1203-1214, 2001.
- [31] Shigley J. E., "Mechanical engineering design" 5th edition, ISBN 0-07-100 607-9, 1989